Localization of Brain Tumors from Digital Magnetic Resonance Images (MRIs)

Maryam Parhizkar

***Abstract*—Brain tumors have high morbidity and poor prognosis. Magnetic Resonance Imaging (MRI) is a non-invasive, non-destructive tool commonly used for early detection of tumors, which is essential for diagnosis, treatment and rehabilitation [1]. Automatic, computer-aided tumor detection from digital MRIs can significantly improve the process. This work aims to develop an algorithm to automatically segment brain MR images and detect tumors. The images used for this project are sourced from a publicly available dataset of T1-weighted contrast-enhanced MR images [2], [3]. The MRIs are pre-processed, before applying a fuzzy c-means clustering (FCM) algorithm to segment the overall image. Finally, in post-processing, the segment identified as the tumor is cleaned by applying connected-component analysis and morphological dilation. This method is evaluated by comparing the detected tumor section to ground truths available in the dataset. Overall, this method found the tumor with high sensitivity (84%) and specificity (95%), but low IoU (Intersection-over-Union: 63%). It performed best detecting meningiomas, moderately well for gliomas, and worst for pituitary tumors.**

I. Introduction

TUMORS can be defined as abnormal growth of cells in the body. Brain tumors are often life-threatening diseases and are a major contributing factor to the global death rate [4]. Detection of the tumor at an early stage can often allow for better treatment and clinical trial options, improving the prognosis, survival and overall quality of life. The common practice in determining brain tumors is to evaluate information acquired from Magnetic Resonance Imaging (MRI) scans [4]–[6]. Physicians and the medical team have to diagnose many patients and segment the tumors manually within the images. Because the brain image contains various tissues, this procedure is often time-consuming and may result in diagnosis errors, as this is highly dependent on the observer's experience.

Computer-aided diagnosis to detect the tumor from the MRI scans with image processing techniques can remarkably reduce the workload and allow for a more standardized diagnosis screening method. Over the years, there have been several studies that attempted to develop accurate tumor area segmentation algorithms that lie in semi and fully automated approaches [5], [7]–[10].

A. Objectives

The primary objective of this work is to develop a simple and automatic approach to segment brain MR images and detect the tumor. For the purposes of this study, we assume the dataset contains only single tumors observable in a transverse MRI image of the brain.

B. Dataset

The images used in this project are from a publicly available dataset of T1-weighted contrast-enhanced MR images [3]. The dataset contains a ground truth mask for each tumor and a label classifying it as a meningioma, glioma or pituitary tumor. This information is beneficial for validating and evaluating the proposed algorithm. Images within the project dataset were constrained such that only axial scans that minimally included orbital sockets were selected. This constraint ensured that a single skull-stripping method could reliably be applied to all scans in the project dataset. The final project dataset includes 21 scans: 7 of each tumor type.

II. Methodology

MRIs are 2D grayscale images that display intensities in the range of 0-255; high-density structures such as bones have higher intensities. The high-level tumor segmentation algorithm is based on implementing a popular segmentation method, Fuzzy C-Means (FCM) clustering. It is an unsupervised learning method rooted in basic image processing concepts. An image is initially segmented into 'c' random clusters and by iterative steps, the degree of membership of each pixel is updated to determine which cluster it belongs to. The details of the FCM clustering are further discussed in the following sections, along with the other processing steps

***Index Terms* — Magnetic Resonance Imaging, MRI, FCM, Fuzzy C-Means Clustering, Image Processing, Automatic Tumor Detection, Brain Tumors, Meningioma, Glioma, Pituitary.**

for this project. All the programming for this project has been performed in Matlab R2020b student edition.

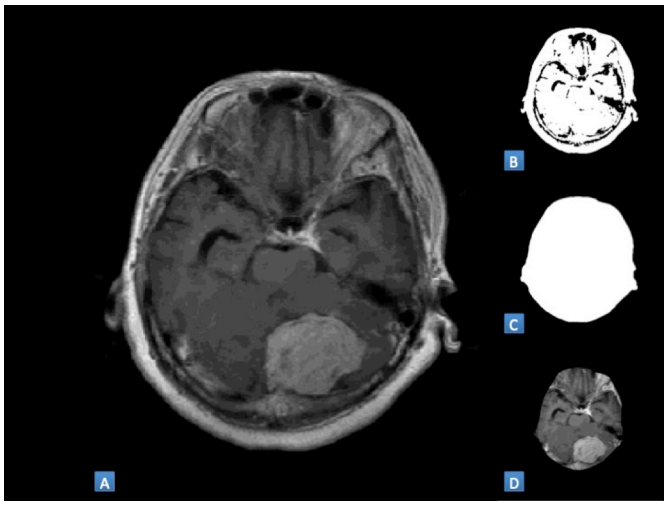

Fig. 1. (A) Typical MRI Image of brain (B) Binarized image showing all structures identified (C) Mask created from all structures (D) Skull-stripped MRI image. An eroded mask from C was applied to A. Contrast-enhancement is performed on this before applying the FCM algorithm

A. Pre-Processing

A typical pre-processing step in image analysis is contrast enhancement. This processing was performed on the MRIs using Matlab's function imadjust; a contrast enhancement method where the image is re-mapped such that 1% of the data is saturated at the low and high intensities from the input dataset. Typically in MRIs of brain tumors, the intensities that indicate skull bones usually overlap with tumor intensities. Therefore, skull portions must be removed to acheive accurate tumor detection [8]. The steps in pre-processing are graphically shown in Figure 1.

The image was binarized with a global threshold that minimized intraclass variance between the black and white pixels to identify the most distinguishable structures within the MRI. As can be seen in the Figure 1.B, some gaps were left between the structures where the intensity was not high enough. In order to create a complete mask, morphological refinement was performed through a process called closing [11]. Closing involves a sequence of two operators, 'dilation' followed by 'erosion' as shown in equations (1) and (2), respectively.

$$A \oplus B = \{Z \in E \mid (B^s)_z \cap A \neq \phi\}$$

… where B^S denotes the symmetric of B (1)

$$A \ominus B = \{Z \in E \mid B_z \subseteq A\}$$

…where B_Z is the translation of B by vector z (2)

The erosion of a binary image A in set Z by a structuring element B is the translation of B that fits the input image, A, entirely. Erosion removes small noise segments from a binarized image while reducing its size. Dilation is the translation of B that intersects with at least one pixel of A. By performing dilation followed by erosion, pepper noise is removed and gaps in bright areas are filled while still maintaining the initial region size. A circular disk shape with a radius of 40 pixels was used, resulting in the mask (Fig. 1.C). This mask was further reduced in size using erosion with a disk radius of 35 pixels to purposefully exclude the outer layer of the identified structure (i.e. the skull). The radius was determined by empirical observation as it was found to be optimal for skull stripping in adult MRIs. This mask was then applied to the image to strip the skull. This pre-processing was performed on all MRIs before FCM clustering was implemented.

B. FCM Clustering

1) Image vectorization

The FCM algorithm expects an array of data points that it will group into clusters. To do this, the 2D MRIs were first converted into a 1D feature vector array with scalar values where each element represents the corresponding pixel intensity. The number of samples equals the number of pixels in a given image.

2) FCM Steps and Cost function

For FCM clustering, with 'c' given clusters, the Euclidean distance of each sample in the feature vector to the cluster centers was determined. Each sample starts as a part of every cluster. The degree of membership of a sample to a given cluster was then iteratively adjusted based on the similarity of the sample and the cluster centers.

$$C_j = \frac{\sum_{i=1}^{N} \mu_{ij}{}^{m} x_i}{\sum_{i=1}^{N} \mu_{ij}{}^{m}} \quad (3)$$

$$\mu_{ij}{}^{m} = \frac{1}{\sum_{k=1}^{C} \left[\frac{|(x_i - c_j)|^2}{|(x_i - c_k)|^2} \right]^{\frac{2}{m-1}}} \quad (4)$$

The cluster centers, C_j, and the membership function, μ_{ij}, were defined as shown in equations (3) and (4). Every pixel had a degree of membership corresponding to each cluster where the total degree of membership across all clusters was equal to one.

The center of the j^{th} cluster was calculated by multiplying the pixel intensity with the corresponding membership function at that step, divided by the summation of all membership functions. This was then used to evaluate the membership function within the iteration, according to equation (4). Here, the Euclidean distance of a pixel from the cluster was divided by its distance with all clusters. This value was summed,

squared and inverted to get the new membership function μ_{ij}. The new membership value was then utilized to adjust the cluster centers in the next iteration.

The goal was to adjust the membership of the samples such that the cost function, J, defined in equation (5) is minimized:

$$J = \sum_{i=1}^{N} \sum_{j=1}^{C} \mu_{ij} \left|(x_i - C_j)\right|^2 \quad (5)$$

In this way, the cluster centers and membership functions were iteratively adjusted until the maximum number of iterations (50 epochs) had been performed. The epoch limit was determined from the available literature and empirical observation. Each sample had 'c' membership degrees, corresponding to each of the c-clusters. The sample was assigned to the cluster with the highest membership degree. Finally, the vector and label would be rescaled to 2D to visualize the final image and segmentation.

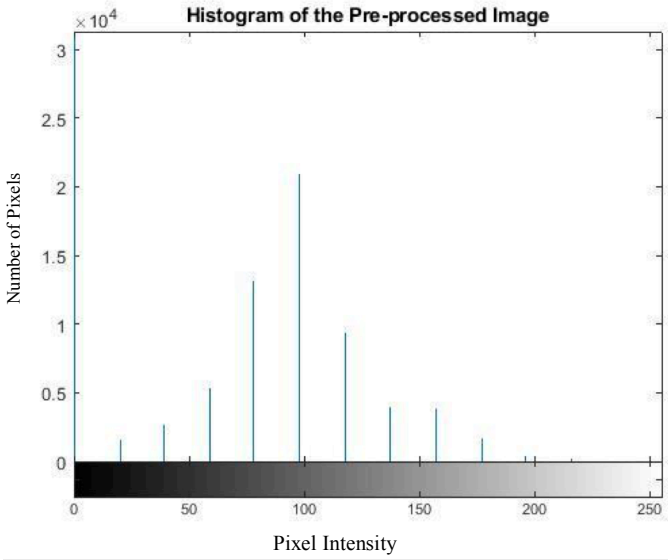

Fig. 2. Histogram of Pre-processed, skull-stripped, MRI of brain structures. The intensities are spread out with more pixels near the lower-intensity regions. Optimal clustering was determined to be between 4-7.

3) Setting Number of Clusters

The number of clusters affects the complexity of the iterative steps: too few clusters would decrease the value of the segmentation, while too many clusters, would mean higher computational costs and undesirable granularity in the final segmentation. In order to determine the appropriate number of clusters, histograms of the MRIs were reviewed (Figure 2).

Examining the MRIs and their histograms, it was evident that the brightest intensities were indicative of tumor tissues within the brain structure. A cluster size of 4-7 seemed appropriate, and so was fixed to 6 and the cluster centers were initialized to zero for all images.

The membership function illustrates the similarity between the sample and the cluster center under consideration. Higher 'm' value increases the degree of 'fuzziness' as it represents the slope of the degree of membership. In this study m was set to two.

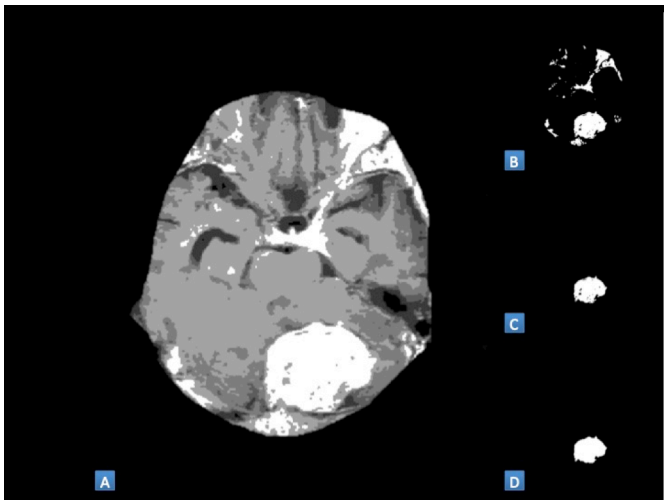

Fig. 3. FCM and Post-Processing steps. (A) The masked, contrast-enhanced input to the FCM algorithm (B) The output region of interest from FCM (C) The largest component of CCA (d) Final identified tumor region

C. Post-Processing

The post-processing steps after the FCM clustering can be seen graphically in Figure 3. As previously mentioned, the brightest intensity pixels often correspond to the tumor region. Therefore, the highest intensity cluster was labeled as the area of interest. This area was further 'cleaned' using connected-component analysis (CCA).

The resulting area of interest from FCM clustering often produced disjointed regions as probable tumor areas (Fig. 3.B). The CCA method compared the labeled pixels and grouped them based on their connectivity to neighboring labeled pixels. This analysis separated the areas of interest into groups of pixels. Small areas were considered noise and were subsequently removed. Since the search was constrained to a single tumor, the largest component identified in the CCA algorithm was identified as the final region of interest (Fig. 3.C). For completeness, a closing operation was performed on this region again to remove any pepper spots and resulted in a whole mask as the 'identified tumor' in 2D space (Fig. 3.D).

D. Evaluation

To evaluate the performance of the proposed method, the outcomes of the algorithm were compared to the ground truth segmentations available within the dataset. This section presents the metrics used to measure the quality of the tumor detection method.

		Actual Class	
		Tumor	Background
Predicted Class	Tumor	TP	FP
	Background	FN	TN

Table. 1. Confusion matrix table setup

The evaluation methods are pixel-based, therefore each pixel is classified into one of four categories. True positive pixels are those correctly classified as part of the tumor and true negative pixels are those correctly classified as non-tumor. On the other hand, false positive pixels are those classified as tumor when they are not and false negative pixels are those classified as non-tumor when they are in fact tumor. These four categories are often represented as part of a confusion matrix, as shown in Table 1.

Various evaluation metrics were computed based on the distribution of values within the confusion matrix. The evaluation methods of interest for this project include: intersection over union (IoU), sensitivity and specificity, shown below in equations (6), (7) and (8). IoU provides an overall sense of how well the algorithm performs by dividing the intersection of the predicted and actual tumors by their union. Furthermore, IoU is robust in cases of significant class imbalance. Sensitivity provides a measure of how well the algorithm does at correctly identifying tumor pixels, and specificity does the same for non-tumor pixels. The combination of these three metrics provides a well-rounded evaluation of the algorithm's performance.

$$IoU = \frac{TP}{TP+FP+FN} \tag{6}$$

$$\mathrm{Se} = \frac{TP}{TP+FN} \tag{7}$$

$$\mathrm{Sp} = \frac{\mathrm{TN}}{\mathrm{TN}+\mathrm{FP}} \tag{8}$$

III. Results

Table 2 provides the average of each evaluation metric observed for all images within the dataset: metrics are also provided for each type of tumor. Figure 4 shows a comparison between a detected tumor region and a ground truth. The results were evaluated quantitatively using the proposed evaluation metrics and qualitatively by visually inspecting the resulting tumor region and ground truth.

	IoU	*Sensitivity*	*Specificity*
Total	*0.629*	*0.841*	*0.954*
Meningiomas	*0.884*	*0.902*	*0.998*
Gliomas	*0.600*	*0.819*	*0.929*
Pituitary	*0.402*	*0.802*	*0.934*

Table. 2. Overall evaluation metrics.

IV. Discussion

Overall, the proposed method had high sensitivity and specificity but a lower than expected IoU score. Since the tumor region is small relative to the rest of the image, the sensitivity value accurately indicates how much of the tumor was correctly classified. The moderate sensitivity value indicates that the algorithm was often successful in classifying tumor pixels as such. Instances of decreased sensitivity were often the result of the algorithm not detecting the tumor or detecting only a small part of the tumor.

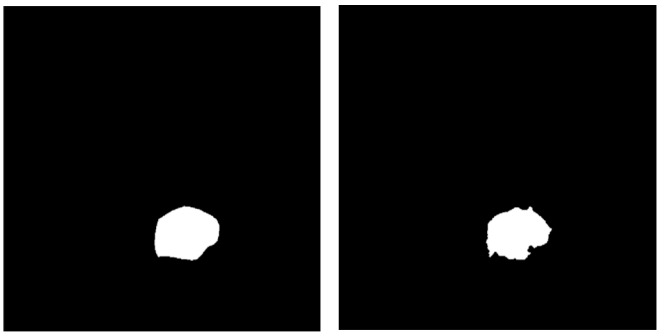

Fig. 4. Ground truth (left) compared against detected tumor (right). This example shows a meningioma tumor-type.

Specificity values are slightly inflated due to the class imbalance between tumor and non-tumor regions. It is also the reason we can observe high specificity and sensitivity values but a low IoU. In order to significantly decrease the specificity value, a considerable portion of the non-tumor region would need to be miss-classified. This miss-classification would lead to a relatively minor decrease in specificity but will dramatically impact the IoU score. Cases of lower specificity and consequentially low IoU were often the result of the algorithm selecting an area much larger than the tumor itself.

Further analysis indicates that the developed method performs better for specific types of tumors than for others. Of the tumor subclasses, the algorithm performed the best for meningiomas. The tumors in this class were notably larger and brighter. Developing in the membranes, these tumors are often surrounded by less dense substances (e.g. synovial fluid), allowing for noticeable edge detection. These characteristics of the tumors in the MRIs were favorable for the developed algorithm, which relied on a high contrast between the tumor and surrounding brain matter and the assumption of relatively large tumor size.

The algorithm performed slightly worse for gliomas. Many of the sample images in this class had bright borders that did not always wholly enclose the dark interior. Often the algorithm would detect these bright borders and group them with neighboring regions of higher intensity. As a result, the detected tumor would partially enclose the actual tumor along with significant non-tumor area. This type of selection would often be either partially selected in the final detected tumor or dropped in the CCA step. This behavior is reflected in the glioma evaluation metrics, where we observe the lowest specificity score and an average sensitivity score.

The algorithm performed the worst for pituitary tumors. Visual observation of the MRIs revealed that these tumors were typically bright but small. This

characteristic led to a classification dichotomy where the algorithm would either detect the tumor almost perfectly or fail altogether. The root of the problem may be in the logic of the CCA step, where only the largest area was being selected as the possible tumor. In such cases adjusting the CCA logic to consider factors other than the size of the component may be beneficial. A workaround has not been developed but can be speculated to include another feature that provides additional weight to the components in the CCA step. This information could be pooled from the membership degree or secondary clusters from the FCM portion to provide additional weights during CCA.

V. Conclusion

The proposed FCM based tumor detection algorithm from MRI images was developed and implemented successfully on 21 MRIs. It performed well when the tumors were large, homogeneous masses, but struggled when the tumor sizes were small. Further developments may include modifications to detect secondary tumors and including more parameters in the segmentation (eg. texture, shape, perimeter, etc.). Additional improvements could be made to account for tumor masses of varying tissue density, which appear on MRIs with non-homogeneous intensities. This improvement may require more complex segmentation methods to accurately identify the edges of such tumors. A possible solution may involve modifying the tumor detection to a semi-automatic method; A user may be asked to define the boundaries of a section of the MRI to segment, instead of the fully-automatic method implemented here. This solution would also remove the need for skull-stripping and allow the FCM algorithm to become more refined and possibly even detect non-homogeneous tumors. Finally, this algorithm could be improved to make use of the vast anatomical detail embedded in MRIs by including information from more than one plane. This improvement could introduce other parameters such as voxels to the feature space to detect volumetric tumor boundaries in 3D space – this improvement could be beneficial for targeted treatment or tumor resection.

References

[1] P. Rangne, P. R. M. Bhombe, and P. A. S. Welankiwar, "Brain Tumor Extraction from MRI Images Using MATLAB," *Int. J. Innov. Sci. Res. Technol.*, vol. 5, no. 9, pp. 436–439, 2020, doi: 10.38124/ijisrt20sep102.

[2] J. Cheng *et al.*, "Enhanced performance of brain tumor classification via tumor region augmentation and partition," *PLoS One*, vol. 10, no. 10, pp. 1–14, 2015, doi: 10.1371/journal.pone.0140381.

[3] J. Cheng, "brain tumor dataset," *figshare*, 2017. https://doi.org/10.6084/m9.figshare.1512427.v5 (accessed Apr. 02, 2017).

[4] D. S. S. K. Vipin Y. Borole, Sunil S. Nimbhore, "Image Processing Techniques for Brain Tumor Detection: A Review," *Int. J. Emerg. Trends Technol. Comput. Sci. Web*, vol. 4, no. 5, pp. 28–32, 2015, [Online]. Available: http://www.ijettcs.org/Volume4Issue5(2)/IJETTCS-2015-10-01-7.pdf.

[5] V. Velusamy, M. Karnan, R. Shivakumar, and N. Nandhagopal, "Enhancement Techniques and Methods for MRI- A Review," *Ijcsit*, vol. 5, no. 1, pp. 397–403, 2014.

[6] K. ABID, "BRAIN TUMOR DETECTION USING MRI AND CT IMAGE," *i-manager's Journal on Image Processing*, vol. 7, no. 3. iManager Publications, p. 25, 2020, doi: 10.26634/jip.7.3.17141.

[7] M. Angulakshmi and G. G. Lakshmi Priya, "Automated brain tumour segmentation techniques— A review," *Int. J. Imaging Syst. Technol.*, vol. 27, no. 1, pp. 66–77, 2017, doi: 10.1002/ima.22211.

[8] P. Kalavathi and V. B. S. Prasath, "Methods on Skull Stripping of MRI Head Scan Images—a Review," *J. Digit. Imaging*, vol. 29, no. 3, pp. 365–379, 2016, doi: 10.1007/s10278-015-9847-8.

[9] R. R. Laddha and S. A. Ladhake, "A Review on Brain Tumor Detection Using Segmentation And Threshold Operations," *Int. J. Comput. Sci. Inf. Technol.*, vol. 5, no. 1, pp. 607–611, 2014.

[10] S. Vaishali, K. K. Rao, and G. V. S. Rao, "A review on noise reduction methods for brain MRI images," *Int. Conf. Signal Process. Commun. Eng. Syst. - Proc. SPACES 2015, Assoc. with IEEE*, no. March, pp. 363–365, 2015, doi: 10.1109/SPACES.2015.7058284.

[11] M. Sonka, V. Hlavac, and R. Boyle, *Image processing, analysis, and machine vision*. Cengage Learning, 2014.